Long-Term Evolution of Broken Wakefields in Finite-Radius Plasmas

K. V. Lotov and A. P. Sosedkin
Budker Institute of Nuclear Physics SB RAS, 630090 Novosibirsk, Russia and Novosibirsk State University, 630090 Novosibirsk, Russia

A. V. Petrenko
Budker Institute of Nuclear Physics SB RAS, 630090 Novosibirsk, Russia and CERN, CH-1211 Geneva 23, Switzerland

(Received 6 February 2014; published 14 May 2014)

A novel effect of fast heating and charging a finite-radius plasma is discovered in the context of plasma wakefield acceleration. As the plasma wave breaks, most of its energy is transferred to plasma electrons. The electrons gain substantial transverse momentum and escape the plasma radially, which gives rise to a strong charge-separation electric field and azimuthal magnetic field around the plasma. The slowly varying field structure is preserved for hundreds of wakefield periods and contains (together with hot electrons) up to 80% of the initial wakefield energy.

DOI: 10.1103/PhysRevLett.112.194801 PACS numbers: 41.75.Lx, 52.40.Mj, 52.50.Gj

Acceleration of charged particles in plasmas, or plasma wakefield acceleration, is currently a hot field of research [1–4]. A plasma can stand electric fields orders of magnitude stronger than those available in metallic or dielectric structures, and this ability is already well proven experimentally [5,6]. The strength of the electric field in plasma waves is typically limited by the so-called wave breaking field $E_0 = mc\omega_p/e$, where m is the electron mass, c is the light velocity, e is the elementary charge, and $\omega_p = \sqrt{4\pi n_0 e^2/m}$ is the plasma frequency determined by the plasma density n_0. In other words, the energy density of the plasma wave ($\sim E_0^2/8\pi$) can be as high as the rest energy of plasma electrons.

The great majority of investigations is concentrated on either the creation or immediate use of this huge energy density. The long-term evolution of plasma waves at this parameter range has not received much attention. The available studies are focused on the dynamics of plasma ions [7–11], the turbulization of the wave [8,10,12], the creation of solitonlike structures [13–15], or the generation of a magnetic field [16]. Here, we report on the novel aspect of plasma wake behavior, which is related to fast charging of the plasma column and heating of plasma electrons.

The essence of the effect is the following. The plasma wave driven to the nonlinear regime breaks soon after reaching the maximum field amplitude. The released wave energy is quickly converted into kinetic energy of plasma electrons. The electrons gain high transverse momenta and escape radially from the wakefield region. If the plasma has a finite radius of several c/ω_p and a sharp boundary, then there are not enough cold electrons to replace hot electrons escaping the plasma, at least for the time needed for ionizing the surrounding gas. The uncompensated charge of plasma ions creates the strong radial electric field, which in turn keeps most of the hot electrons near the plasma. The escaping electrons predominantly move forward in the laboratory frame and take away some negative current from the plasma. The compensating positive current thus appears in the plasma and creates a strong azimuthal magnetic field around the plasma.

The effect has an intimate connection with the target normal sheath acceleration mechanism of ion acceleration [17,18]. The difference is in the geometric configuration of fields and in the presence of plasma waves as an intermediate energy carrier. As a sharp boundary is usual for plasmas created by short laser pulses via the tunnel ionization mechanism, the effect is quite universal and can be observed in various setups.

Fast heating and charging of the plasma were discovered in the context of the Advanced Wakefield Experiment (AWAKE) project [19–22] aimed at the first experimental demonstration of the proton-driven plasma wakefield acceleration [23,24]. We therefore use this configuration for detailed study of the effect, and after that, discuss the more common case of laser-driven acceleration.

To excite the wakefield efficiently, an initially long proton bunch in AWAKE is transformed into a train of short equally spaced microbunches by the self-modulation instability [25–27]. A small precursor is needed to seed the proper instability mode and to speed up the growth of the self-modulation [28–30]. The instability is seeded and controlled by the copropagating laser pulse, which instantly creates the plasma by quick ionization of highly uniform [31] neutral gas. The plasma has a finite radius of several c/ω_p and a sharp boundary [32]. The plasma wave driven by the train of microbunches breaks soon after reaching the maximum field amplitude of about $0.4E_0$ [33]. If properly injected [34,35] near the maximum of the grown wakefield, witness electrons can be accelerated with a sub-GeV/m rate to the energy of about 2 GeV. With the use of higher-energy drivers and fine control of the plasma density profile

[36], this method is capable of producing multi-TeV electrons in a single accelerating stage [37].

To study the effect, we use the quasistatic axisymmetric $2d3v$ code LCODE with the kinetic solver for plasma electrons, plasma ions, and beam protons [38–40]. We use cylindrical coordinates (r, φ, z) with the z axis as the direction of beam propagation and the time $\tau = t - z/c$ measured from the onset of wave excitation. The applicability of the quasistatic approximation to studies of long beams is justified in Ref. [41]. The beam and plasma parameters correspond to the baseline parameter set of the AWAKE experiment [20,21]. Here, the 400 GeV proton beam initially focused to 0.2 mm must propagate through the highly uniform rubidium plasma of length $L_{\max} = 10$ m and density $n_0 = 7 \times 10^{14}$ cm^{-3} ($c/\omega_p = 0.2$ mm). The beam contains 3×10^{11} protons and is 12 cm long (root-mean-square half-width). Along the first four meters, the beam fully self-modulates; along the following six meters, the beam creates strong wakefields and accelerates externally injected test electrons. The expected plasma radius [32] can be approximated as

$$r_p = 5c/\omega_p(1.5 - 0.5z/L_{\max}). \quad (1)$$

As a measure of the wakefield amplitude, we take local $\Phi_m(z,\tau)$ and absolute $\Phi_{\max}(z)$ extrema of the dimensionless wakefield potential $\Phi(z,\tau)$ on the axis:

$$\Phi(z,\tau) = \frac{\omega_p}{E_0}\int_{-\infty}^{\tau} E_z(z,\tau')d\tau', \quad (2)$$

where E_z is the on-axis electric field. To be exact, the potential should be obtained from E_z by spatial integration, but the quantity [Eq. (2)] is close to the potential as soon as the quasistatic approximation is valid. The wakefield potential is more noise resistant than E_z and contains information on the focusing properties of plasma waves in an easy-to-view form. The function $\Phi_m(z,\tau)$ is the envelope of the oscillating function $\Phi(z,\tau)$. The function $\Phi_{\max}(z)$ is the absolute maximum of $\Phi_m(z,\tau)$ taken over all τ for a fixed z. Although the studied examples are based on realistic experimental setups, we will formulate the results in the dimensionless form wherever reasonable.

First, we note that at these parameters, neither the finite plasma radius r_p itself nor its linear variation with length has any significant effect on the amplitude of the excited wave (Fig. 1). The visible difference of maximum amplitudes is due to specific characters of wave breaking near the axis and does not result from different conditions of wave excitation [Fig. 2(a)]. Plasma charging is best observed at the time of the strongest driver modulation. This place is marked by the cross in Fig. 1.

From the time dependence of the wakefield potential amplitude at $z = 4$ m [Fig. 2(a)], we see that the wave breaks at $\tau \approx 700\omega_p^{-1}$ in both finite-radius and infinite plasmas.

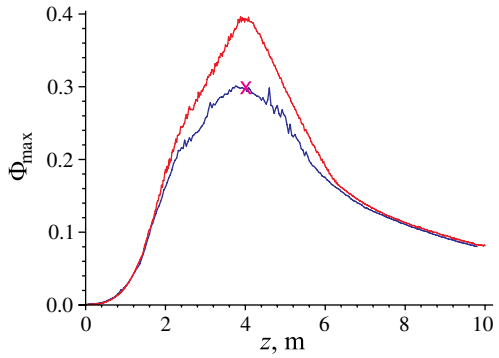

FIG. 1 (color online). Simulated maximum wakefield amplitude versus the propagation distance for infinite (upper line) and finite-radius (lower line) plasmas for parameters of the AWAKE experiments.

Soon after that, the slowly varying radial electric field E_r and azimuthal magnetic field B_ϕ appear in the finite-radius case [Figs. 2(b) and 2(d)]. These fields reach their maximum values near the plasma boundary. To separate them from the oscillating wakefields, we average the actual fields over one plasma period ($2\pi\omega_p^{-1}$). In the infinite plasma, no strong average field appears [Figs. 2(c) and 2(e)].

The trajectories of plasma electrons responsible for charging the plasma are shown in Fig. 2(f). The high-energy electrons appear at the time of wave breaking. The first of them dart directly to the outer wall located at $r_{\max} = 20c/\omega_p$ and carry out the negative charge. Later produced fast electrons are confined by the generated electric field but still make long radial excursions. In the code, as soon as an electron hits the wall, it is reflected back inelastically with some low energy. This models the emission of secondary electrons. The secondary electrons are pulled back to the plasma and also participate in the formation of the electron halo between the plasma and the wall. In the infinite plasma, high-energy electrons are also generated as the wave breaks [Fig. 2(g)], but the bulk of cold electrons fully compensate the escaping charge. Correspondingly, no secondary electrons are pulled back toward the plasma axis.

Figure 3 shows the energy distribution of the halo electrons at the stage of established equilibrium and the shape of the electrostatic potential

$$W_r(r) = e\int_r^{r_{\max}} \langle E_r\rangle dr, \quad (3)$$

where the angled brackets denote time averaging over the interval $2\pi\omega_p^{-1}$. We see that both the maximum electron energy and the depth of the potential well for them are about 200 keV. This corresponds to electric fields as strong as 200 MV/m at the plasma boundary.

As follows from the mechanism of field formation, only the highest-energy or earliest born fast electrons interact with the outer wall. Consequently, if $r_{\max} \gg r_p$, the field structure weakly depends on $r_{\max}$, and simulations confirm this fact.

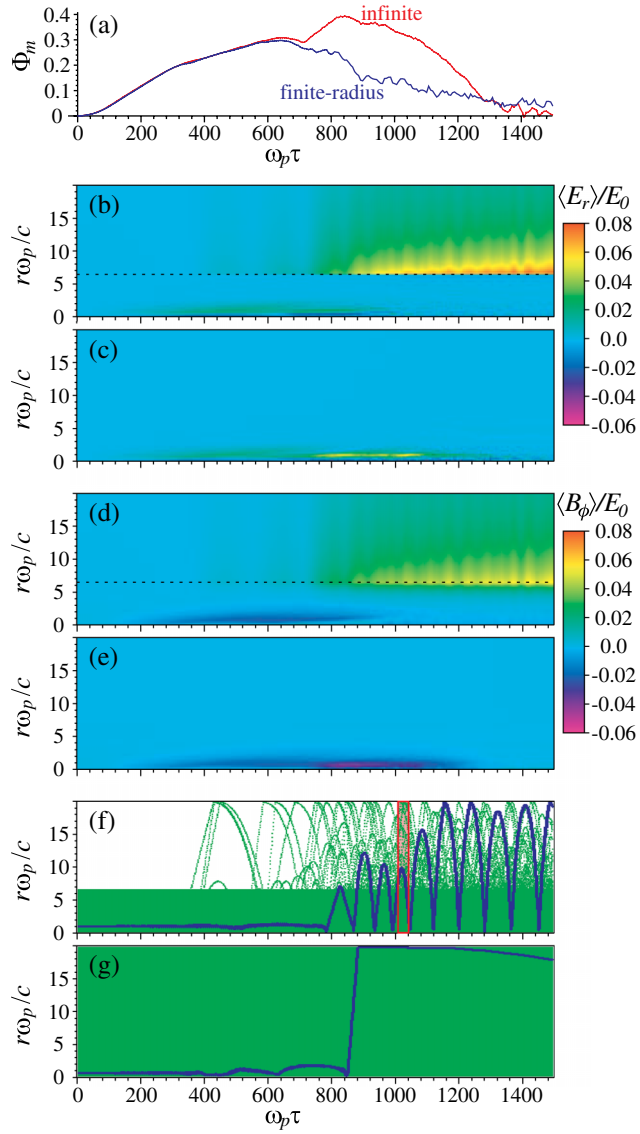

FIG. 2 (color online). Time dependence of the wakefield amplitude for (a) finite-radius and infinite plasmas, the spatial distribution of (b),(c) the period-averaged radial electric field $\langle E_r\rangle$ and (d),(e) the azimuthal magnetic field $\langle B_\phi\rangle$, and (f),(g) trajectories of selected plasma electrons in the comoving window at the stage of the fully modulated beam (at $z = 4$ m) for (b),(d), (f) finite-radius and (c),(e),(g) infinite plasmas. In pictures (f) and (g), one trajectory is shown in blue (darker), while the others are shown in green (lighter). The horizontal dashed lines in (b) and (d) show the plasma radius. The narrow rectangle in (f) shows the area characterized in Fig. 3.

The average longitudinal motion of plasma electrons is best viewed on the map of electron velocities (Fig. 4). The electron halo predominantly moves forward, while the compensating current is concentrated in the area of width $\sim c/\omega_p$ near the plasma boundary. Correspondingly, the magnetic field penetrates the outer plasma region [Fig. 2(d)], unlike the electric field, which is sharply screened by the surface charge [Fig. 2(b)]. This field behavior resembles

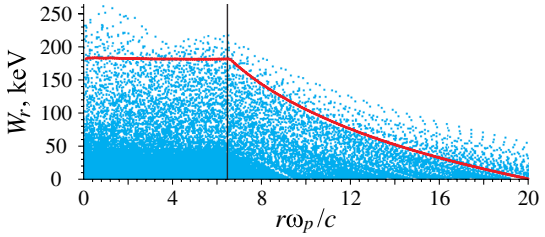

FIG. 3 (color online). Energy of plasma electrons versus their radial position (dots) and the radial dependence of the electrostatic potential $W_r(r)$ (red line) at the stage of established equilibrium ($\tau = 1120\omega_p^{-1}$, $z = 4$ m). The vertical black line shows the plasma boundary.

the penetration of a slowly varying electromagnetic wave into the plasma in classical electrodynamics.

The overall action of electric and magnetic fields on axially moving relativistic particles is characterized by the wakefield potential Φ (Fig. 5), which has an off-axis slowly varying spike, i.e., the potential well for electrons. The spike is located exactly at the plasma boundary, so its location can be controlled by changing the plasma radius. The height of the off-axis spike is comparable with on-axis potential oscillations caused by residual plasma wakefields [Fig. 5(b)]. However, the energy stored in slowly varying fields is much greater than that in plasma oscillations due to the geometrical factor (since the off-axis area is larger).

The energy balance in the system can be quantitatively described by the energy flux Ψ in the light-velocity frame [42]:

$$\Psi = \int_0^\infty \left[\sum_j m_j c^2(\gamma_j - 1)(c - v_{j,z}) + \frac{c}{8\pi}(E^2 + B^2) - \frac{c}{4\pi}(E_r B_\varphi - E_\varphi B_r)\right] 2\pi r dr, \quad (4)$$

where m_j, $\vec{v}_j$, and γ_j are the mass, velocity, and relativistic factor of individual plasma particles; the sum is over plasma particles in a unit volume. The energy flux Ψ changes as the current j_{bz} of the proton beam works against the wakefield:

$$\frac{\partial \Psi}{\partial \tau} = -c\int_0^\infty j_{bz} E_z 2\pi r dr - cQ, \quad (5)$$

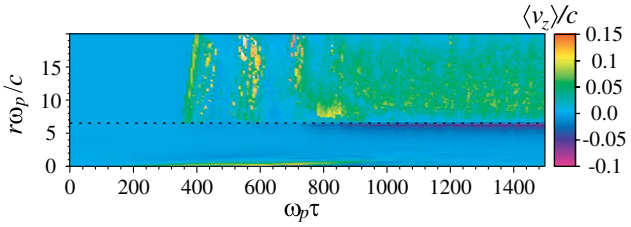

FIG. 4 (color online). Period-averaged velocity of plasma electrons at $z = 4$ m. The horizontal dashed line shows the plasma radius.

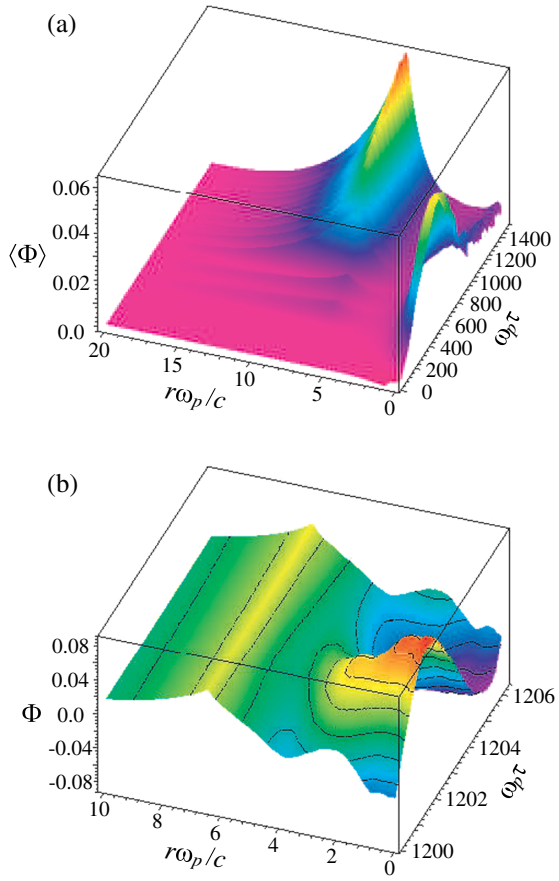

FIG. 5 (color online). The wakefield potential at $z = 4$ m: (a) the period-averaged slowly evolving part and (b) the one-period fragment showing the oscillating part.

where Q is the power absorbed by a unit length of the wall. Analyzing different terms in Eq. (4) allows us to separate the energy accumulated in particles and fields. We can find that in the finite-radius plasma, 82% of the energy left by the driver remains in the plasma; 17% remains in the fields, and 65% remains in the motion of plasma electrons. In contrast, in the infinite plasma, about 15% of the energy remains in the plasma after wave breaking and only 5% is the field energy. The latter number gives us the estimate for the energy that remains in residual wakefields (~10%), as the field energy is approximately half of the plasma wave energy. In the above energy balances, the energy is lost to the walls. Other loss mechanisms such as radiative losses and the ionization of neutral particles are small and not taken into account.

The lifetime of the formed field structure can be limited either by ion motion or by ionization of the surrounding gas. The time it takes for the electric field to displace a plasma ion of the mass M_i is of the order of

$$\tau_{\text{ion}} = \omega_p^{-1}\sqrt{M_i E_0/(m\langle E_r\rangle)} \tag{6}$$

or 1.2 ns (300 wave periods) for the considered plasma and $\langle E_r\rangle = 0.05E_0$. After that time, ion motion comes into play and takes the energy from fields and hot electrons in a way similar to the target normal sheath acceleration mechanism.

The ionization time is determined by the cross section of electron impact ionization. For the lower estimate of the electron energy (1 keV), typical values of the ionization cross section σ_i range from 15 Å^2 for hydrogen and helium to several Å^2 for heavier elements [43]. For the rubidium plasma ($\sigma_i \approx 1.5$ Å^2 [44]), this corresponds to the mean free path $\lambda_i = 1/(n\sigma_i) \sim 10$ cm and ionization time ~5 ns. Since, for nonrelativistic electrons with energies $W_E \gg 100$ eV, the ionization cross section scales as W_E^{-1} [45] and most outer electrons have energies well above 1 keV (Fig. 3), the average ionization time is even longer and much longer than the ion response time. Thus, the lifetime of the slowly varying fields is determined by ion motion and is as long as hundreds of plasma periods.

The physical effects responsible for the formation of slowly varying electromagnetic fields and the cloud of hot electrons are not specific to proton drivers and can also be reproduced with a simpler setup. To illustrate this, we simulate long-term evolution of the wakefields created by a short laser pulse in a hydrogen plasma of the radius $r_p = 3.5c/\omega_p$. The pulse shape is defined by the normalized vector potential $\vec{a} = e\vec{A}/(mc^2)$ squared:

$$|a|^2 = \frac{a_0^2 e^{-r^2/\sigma_r^2}}{2}\left[1 + \cos\left(\frac{\sqrt{\pi}c(\tau-\tau_c)}{\sigma_z\sqrt{2}}\right)\right], \tag{7}$$
$$|\tau - \tau_c| < \sigma_z\sqrt{2\pi}/c,$$

with $a_0 = 5$, $\sigma_r = c/\omega_p$, $\sigma_z = \sqrt{2}c/\omega_p$, and $\tau_c = 3.55\omega_p^{-1}$. The wall is located at $r_{\max} = 40c/\omega_p$.

All the above discussed features are reproduced with this driver, namely, a slowly varying radial electric field around the plasma (~$0.5E_0$), a slowly varying azimuthal magnetic field penetrating outer plasma layers (also ~$0.5E_0$), a smooth hill of the wakefield potential (Fig. 6), and a cloud of hot electrons around the plasma. The energy balance here is the following: 80% of the energy delivered by the driver remains with the plasma, 13% remains in the electromagnetic fields, and 67% is the kinetic energy of plasma particles.

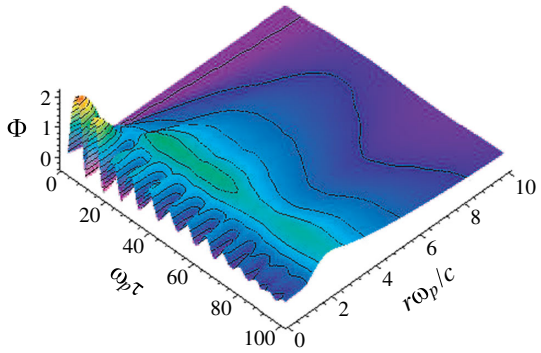

FIG. 6 (color online). The wakefield potential produced by the short laser pulse.

To conclude, we discovered that the energy stored in the plasma in the form of a high-amplitude plasma wave is eventually converted to the thermal energy of a small fraction of plasma electrons. If the plasma has a finite radius, then most of this energy remains near the plasma, since fast electrons create a strong charge-separation electric field and are kept by this field around plasma ions. Because of the specific nature of wave breaking, a strong azimuthal magnetic field also appears around the plasma. The tubular potential well (or hill) associated with these fields may find use for focusing, concentrating, or scattering relativistic particles. The location of the potential spike can be controlled by changing the plasma radius as the two coincide. Perhaps, further optimization for a particular need may result in even stronger or smoother fields or higher efficiency of the energy transfer from the drive beam to the slowly varying field structure.

This work was supported by the Ministry of Education and Science of Russia, Siberian Supercomputer Center SB RAS, and RFBR Grant No. 14-02-00294.

[1] S. Corde, K. Ta Phuoc, G. Lambert, R. Fitour, V. Malka, A. Rousse, A. Beck, and E. Lefebvre, Rev. Mod. Phys. **85**, 1 (2013).
[2] V. Malka, Phys. Plasmas **19**, 055501 (2012).
[3] E. Esarey, C. B. Schroeder, and W. P. Leemans, Rev. Mod. Phys. **81**, 1229 (2009).
[4] C. Joshi, Phys. Plasmas **14**, 055501 (2007).
[5] I. Blumenfeld, C. E. Clayton, F.-J. Decker, M. J. Hogan, C. Huang, R. Ischebeck, R. Iverson, C. Joshi, T. Katsouleas, N. Kirby, W. Lu, K. A. Marsh, W. B. Mori, P. Muggli, E. Oz, R. H. Siemann, D. Walz, and M. Zhou, Nature (London) **445**, 741 (2007).
[6] W. P. Leemans, B. Nagler, A. J. Gonsalves, Cs. Toth, K. Nakamura, C. G. R. Geddes, E. Esarey, C. B. Schroeder, and S. M. Hooker, Nat. Phys. **2**, 696 (2006).
[7] L. M. Gorbunov, P. Mora, R. R. Ramazashvili, and A. A. Solodov, Phys. Plasmas **7**, 375 (2000).
[8] L. M. Gorbunov, P. Mora, and A. A. Solodov, Phys. Rev. Lett. **86**, 3332 (2001).
[9] L. M. Gorbunov, P. Mora, and R. R. Ramazashvili, Phys. Rev. E **65**, 036401 (2002).
[10] L. M. Gorbunov, P. Mora, and A. A. Solodov, Phys. Plasmas **10**, 1124 (2003).
[11] J. Vieira, R. A. Fonseca, W. B. Mori, and L. O. Silva, Phys. Rev. Lett. **109**, 145005 (2012).
[12] C. T. Zhou, M. Y. Yu, and X. T. He, Laser Part. Beams **25**, 313 (2007).
[13] S. V. Bulanov, M. Lontano, T. Zh. Esirkepov, F. Pegoraro, and A. M. Pukhov, Phys. Rev. Lett. **76**, 3562 (1996).
[14] S. V. Bulanov, T. Zh. Esirkepov, N. M. Naumova, F. Pegoraro, and V. A. Vshivkov, Phys. Rev. Lett. **82**, 3440 (1999).
[15] Y. Sentoku, T. Zh. Esirkepov, K. Mima, K. Nishihara, F. Califano, F. Pegoraro, H. Sakagami, Y. Kitagawa, N. M. Naumova, and S. V. Bulanov, Phys. Rev. Lett. **83**, 3434 (1999).
[16] L. Gorbunov, P. Mora, and T. M. Antonsen, Jr., Phys. Rev. Lett. **76**, 2495 (1996).
[17] A. Macchi, M. Borghesi, and M. Passoni, Rev. Mod. Phys. **85**, 751 (2013).
[18] H. Daido, M. Nishiuchi, and A. S. Pirozhkov, Rep. Prog. Phys. **75**, 056401 (2012).
[19] AWAKE Collaboration, arXiv:1401.4823 [Plasma Phys. Controlled Fusion (to be published)].
[20] P. Muggli, A. Caldwell, O. Reimann, E. Oz, R. Tarkeshian, C. Bracco, E. Gschwendtner, A. Pardons, K. Lotov, A. Pukhov, M. Wing, S. Mandry, and J. Vieira, in *Proceedings of IPAC2013, Shanghai, China, 2013*, p. 1179, http://accelconf.web.cern.ch/accelconf/IPAC2013/papers/tupea008.pdf.
[21] AWAKE Collaboration, CERN Report No. SPSC-TDR-003, http://cds.cern.ch/record/1537318/files/SPSC-TDR-003.pdf.
[22] C. Bracco, E. Gschwendtner, A. Petrenko, H. Timko, T. Argyropoulos, H. Bartosik, T. Bohl, J. E. Mueller, B. Goddard, M. Meddahi, A. Pardons, E. Shaposhnikova, F. M. Velotti, and H. Vincke, Nucl. Instrum. Methods Phys. Res., Sect. A **740**, 48 (2014).
[23] A. Caldwell, K. Lotov, A. Pukhov, and F. Simon, Nat. Phys. **5**, 363 (2009).
[24] K. V. Lotov, Phys. Rev. ST Accel. Beams **13**, 041301 (2010).
[25] K. V. Lotov, in *Proceedings of the 6th European Particle Accelerator Conference, Stockholm, 1998*, p. 806, http://accelconf.web.cern.ch/AccelConf/e98/PAPERS/MOP12E.PDF
[26] A. Caldwell, K. Lotov, A. Pukhov, and G. Xia, Plasma Phys. Controlled Fusion **53**, 014003 (2011).
[27] N. Kumar, A. Pukhov, and K. Lotov, Phys. Rev. Lett. **104**, 255003 (2010).
[28] K. V. Lotov, G. Z. Lotova, V. I. Lotov, A. Upadhyay, T. Tuckmantel, A. Pukhov, and A. Caldwell, Phys. Rev. ST Accel. Beams **16**, 041301 (2013).
[29] C. B. Schroeder, C. Benedetti, E. Esarey, F. J. Gruner, and W. P. Leemans, Phys. Rev. E **86**, 026402 (2012).
[30] C. B. Schroeder, C. Benedetti, E. Esarey, F. J. Gruner, and W. P. Leemans, Phys. Plasmas **20**, 056704 (2013).
[31] K. V. Lotov, A. Pukhov, and A. Caldwell, Phys. Plasmas **20**, 013102 (2013).
[32] E. Oz and P. Muggli, Nucl. Instrum. Methods Phys. Res., Sect. A **740**, 197 (2014).
[33] K. V. Lotov, Phys. Plasmas **20**, 083119 (2013).
[34] A. Pukhov, N. Kumar, T. Tuckmantel, A. Upadhyay, K. Lotov, P. Muggli, V. Khudik, C. Siemon, and G. Shvets, Phys. Rev. Lett. **107**, 145003 (2011).
[35] K. V. Lotov, J. Plasma Phys. **78**, 455 (2012).
[36] K. V. Lotov, Phys. Plasmas **18**, 024501 (2011).
[37] A. Caldwell and K. V. Lotov, Phys. Plasmas **18**, 103101 (2011).
[38] K. V. Lotov, Phys. Plasmas **5**, 785 (1998).
[39] K. V. Lotov, Phys. Rev. ST Accel. Beams **6**, 061301 (2003).
[40] http://www.inp.nsk.su/~lotov/lcode.
[41] K. V. Lotov, V. I. Maslov, I. N. Onishchenko, and E. N. Svistun, Plasma Phys. Controlled Fusion **52**, 065009 (2010).
[42] K. V. Lotov, Phys. Rev. E **69**, 046405 (2004).
[43] P. L. Bartlett and A. T. Stelbovics, Phys. Rev. A **66**, 012707 (2002).
[44] Y.-K. Kim, J. Migdalek, W. Siegel, and J. Bieron, Phys. Rev. A **57**, 246 (1998).
[45] L. D. Landau and L. M. Lifshitz, *Quantum Mechanics: Non-relativistic Theory* (Elsevier, New York, 2003), 3rd ed.